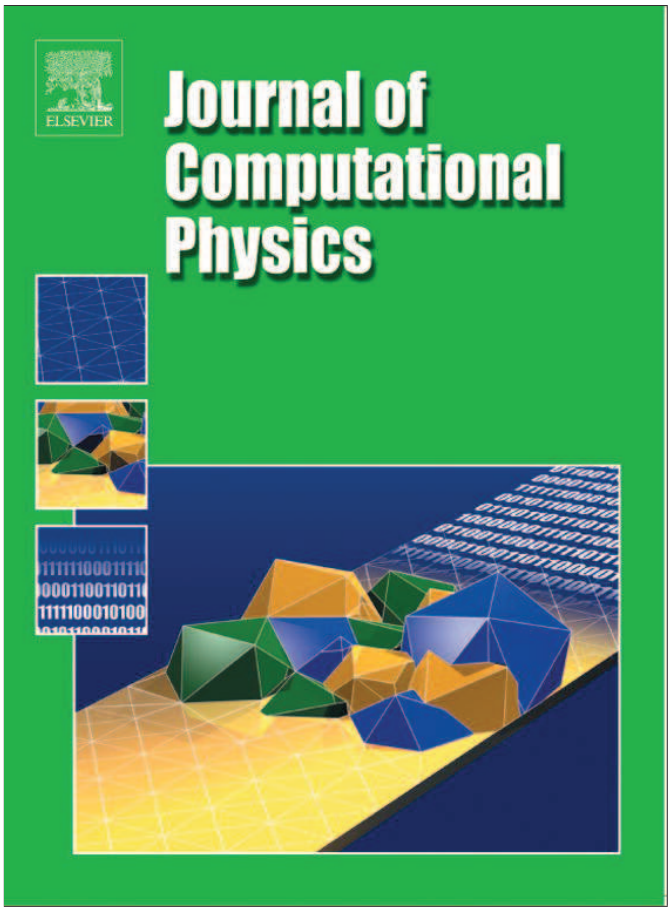

Journal of Computational Physics 251 (2013) 344–363

Contents lists available at SciVerse ScienceDirect

Journal of Computational Physics

journal homepage: www.elsevier.com/locate/jcp

Free molecular collision cross section calculation methods for nanoparticles and complex ions with energy accommodation

Carlos Larriba *, Christopher J. Hogan Jr.

Department of Mechanical Engineering, University of Minnesota, Minneapolis, MN, USA

ARTICLE INFO

Article history:
Received 18 December 2012
Received in revised form 12 May 2013
Accepted 30 May 2013
Available online 15 June 2013

Keywords:
Ion mobility
Collision cross section
Trajectory method
Hard sphere scattering
Induced dipole
Free molecular drag

ABSTRACT

The structures of nanoparticles, macromolecules, and molecular clusters in gas phase environments are often studied via measurement of collision cross sections. To directly compare structure models to measurements, it is hence necessary to have computational techniques available to calculate the collision cross sections of structural models under conditions matching measurements. However, presently available collision cross section methods contain the underlying assumption that collision between gas molecules and structures are completely elastic (gas molecule translational energy conserving) and specular, while experimental evidence suggests that in the most commonly used background gases for measurements, air and molecular nitrogen, gas molecule reemission is largely inelastic (with exchange of energy between vibrational, rotational, and translational modes) and should be treated as diffuse in computations with fixed structural models. In this work, we describe computational techniques to predict the free molecular collision cross sections for fixed structural models of gas phase entities where inelastic and non-specular gas molecule reemission rules can be invoked, and the long range ion-induced dipole (polarization) potential between gas molecules and a charged entity can be considered. Specifically, two calculation procedures are described detail: a diffuse hard sphere scattering (DHSS) method, in which structures are modeled as hard spheres and collision cross sections are calculated for rectilinear trajectories of gas molecules, and a diffuse trajectory method (DTM), in which the assumption of rectilinear trajectories is relaxed and the ion-induced dipole potential is considered. Collision cross section calculations using the DHSS and DTM methods are performed on spheres, models of quasifractal aggregates of varying fractal dimension, and fullerene like structures. Techniques to accelerate DTM calculations by assessing the contribution of grazing gas molecule collisions (gas molecules with altered trajectories by the potential interaction) without tracking grazing trajectories are further discussed. The presented calculation techniques should enable more accurate collision cross section predictions under experimentally relevant conditions than pre-existing approaches, and should enhance the ability of collision cross section measurement schemes to discern the structures of gas phase entities.

* Corresponding author. Tel.: +1 2035038995.
E-mail address: clarriba@umn.edu (C. Larriba).

0021-9991/$ - see front matter © 2013 Elsevier Inc. All rights reserved.
http://dx.doi.org/10.1016/j.jcp.2013.05.038

1. Introduction

Electrical/ion mobility spectrometry has become a standard technique to characterize nanoparticles, macromolecules, and molecular clusters in the gas phase. In general, the electrical/ion mobility (Z_p) and diffusion coefficient (D_p) of an ion traveling at low subsonic speeds in the free molecular regime [1–5], follow the relations:

$$Z_p = \left(\frac{\pi m_{red}}{8kT}\right)^{1/2} \frac{3ze}{4\rho_{gas}\Omega} = D_p ze/kT, \tag{1}$$

where k is Boltzmann's constant, T is the background gas temperature, m_{red} is the reduced mass of the nanoparticles–gas molecule system, and ρ_{gas} is the background gas mass density. As all other parameters in Eq. (1) depend primarily on background gas conditions, experimental measurements in the free molecular regime of charged nanoparticles and ions invariably lead to the inference of the collision cross section (Ω, the orientationally averaged first collision integral). The collision cross section alone quantifies the amount of momentum transferred to a nanoparticle by the impingement of surrounding gas molecules, leading particles of differing size and structure to migrate differentially through a background gas. It is hence essential to develop procedures to calculate collision cross sections for modeled nanoparticle structures, such that experimental measurements can be compared directly to models, or to structures inferred via experimental techniques [6].

There have been considerable efforts made prior along these lines, beginning with the theoretical studies of Langevin [7], Cunningham [8], and Lenard [9] in the early 20th century, and the subsequent kinetic theory proposed by Epstein [10] in an attempt to match the experimental measurements of Millikan [11,12] of spherical oil drops in a diatomic gas. With the exceptions of the analyses by Langevin and Lenard, these efforts focused specifically on spherical particles substantially larger than surrounding gas molecules, for which long range potential interactions between nanoparticles and gas molecules (ion-induced dipole interactions [13]) are negligibly small. A key result from these studies is that for predictions to fall in line with the Millikan measurements as well as with more recent measurements on nanoparticles [14–22], energy accommodation and non-specular gas molecule scattering between impinging gas molecules and particles must be considered, i.e. neither is gas-molecule translational kinetic energy necessarily conserved during collision, nor are gas molecules necessarily reemitted from the surface of a particle at the specular angle.

Subsequent notable analysis of momentum transfer by Chan and Dahneke [23], Garcia-Ybarra and Rosner [24], Rosner et al. [25], Meakin et al. [26], Fernandez de la Mora [27], and Zurita-Gotor [28] has revealed the difficulty of calculating collision cross sections for complex molecular structures theoretically; only convex symmetric structures are easily tractable, due to the mathematical complexity of the non-linear (or linearized by Chapman–Enskog [29] expansion) Maxwell Boltzmann integro-differential equation and to the associated boundary conditions on the particle surface. Accordingly, Chan and Dahneke [23], developed a Monte Carlo algorithm to predict the collision cross section of straight chains of spheres, where elements with parasitic drag coefficients (scattering and concave effects) were calculated separately and then added together. This approach circumvents the need to solve the integro-differential equations directly, and later Nakamura and Hidaka [30] as well as Mackowski [31] employed a similar momentum transfer algorithm to predict the drag and thermophoretic forces of quasifractal aggregate nanoparticles.

In a separate line of research, focusing not on matching the results of Millikan's oil drop experiments (or subsequent related measurements) but rather on direct mobility measurements of gas phase ions of similar size to gas molecules themselves, Mason and McDaniel [1,32] also developed numerical algorithms for collision cross section calculation. Their approach can consider complex, non-spherical nanoparticle shapes and short-range potentials interactions. These methods were adapted by Li and Wang [33,34] for calculation of the collision cross sections of spherical nanoparticles, considering both energy accommodation during gas molecule impingement and the Rudyak–Krasnolutski potential interaction [35] between particles and gas molecules. Moreover, Jarrold and co-workers have developed MOBCAL [13,36,37] based upon these methods, which is a suite of algorithms used to calculate collision cross sections from atomic models. MOBCAL enables calculation of the cross sectional integral in three different manners: (1) the projected-area (PA) approximation, in which the orientationally averaged projected area of a structure is equated with its collision cross section, (2) elastic/exact hard sphere scattering (EHSS) calculations [36], in which gas molecules are assumed to have elastic (translational kinetic energy-conserving) and specular collisions with hard-sphere modeled atoms of a structure, and (3) trajectory (TM) method calculations in which Lennard–Jones potentials between gas molecules and atoms within a structure are considered (with the elastic, specular collision assumption maintained) [13]. In the examination of small (several hundred to several thousand Daltons in mass) ions in He background gas [38,39], collision cross sections predicted with the latter two procedures agree well with experimentally measured collision cross sections, with particularly good agreement found between measurements and TM predictions.

In recent examinations of both ambient [40] and biologically derived nanoparticles/ions [41] (the two most frequently studied systems of charged entities immersed in a gaseous medium), helium and monoatomic gases have been used less frequently for measurements of charged nanoparticles and ions than have more abundantly available diatomic gases. The MOBCAL suite of algorithms has hence been applied for predictions of collision cross sections not only in helium background gas [38,39,42], but also in a number of studies in diatomic gas studies [41,43]. However, from the wealth of experimental measurements now available [14–22], it has become clear that the specular, elastic collision model predictions which are intrinsic to MOBCAL do not agree with measurements in diatomic gases; hence without modification, MOBCAL calculations are not appropriate for comparison to diatomic bath gas measurements. Attempts to modify MOBCAL for diatomic gas calculations

have been made by Kim and co-workers [44–46], though the result is computationally not feasible for application to all-atom models of nanoparticles larger than tens of atoms. Further, for sufficiently small nanoparticles, long range ion-induced dipole interactions must be accounted for in collision cross section calculations and, pending the inclusion of such interactions, it has not yet been shown that the methods of Mason and McDaniel are applicable.

Regrettably, the development of collision cross section calculation methods which can consider energy accommodation upon collisions and which agree with experimental measurements of nanoparticles in diatomic gases has stalled in recent years, and a method to predict nanoparticle collision cross sections efficiently considering finite sized gas molecules, complex nanoparticle structures, long range potential interactions, and energy accommodation during collision, is hitherto unavailable. Therefore, our purpose in this work is to develop a suite of algorithms to calculate collision cross sections considering all of these influences. These algorithms build upon the work of Epstein [10] as well as Chan and Dahneke [23] and, in a parallel manner to the three algorithms incorporated into MOBCAL, we also describe three algorithms for collision cross section calculation, ranging in level of detail from projected area approximations up to gas molecule trajectory calculations with detailed nanoparticle structures and non-specular gas molecule-particle collisions. We note that unlike MOBCAL, which provides three seemingly distinct collision cross section predictions, these algorithms are interrelated and will lead to similar predictions (albeit with increasing accuracy for calculations with greater detail). Moreover, in the presented algorithms full momentum transfer is calculated, allowing for the possibility of real gas-molecule and gas–gas interactions for large scale simulations [47] as well as bulk velocity considerations.

2. Theoretical and numerical approach

2.1. Collision cross section calculation procedures

2.1.1. Method descriptions

We propose that the collision cross section for a nanoparticle, molecular cluster, molecule, or ion migrating in a background gas can be calculated with one of the three following computational methods, noted in order of increasing complexity and detail:

(1) *The projected area (PA) method.* In the *PA* method, the orientationally averaged projected area is determined for the structure of interest accounting for gas molecule-structure interaction. To do so, the atoms or base units of the structure as well as the gas molecule are given prescribed hard sphere radii. Calculations of this type are discussed elsewhere [37,48–51] and are not described in detail here. In prior *PA* methods, the orientationally averaged projected area itself is treated as a first approximation to the collision cross section [43,52]. However, it is clear that this approximation would only apply in instances where (a) the structure under examination is sufficiently convex, such that multiple collisions by a gas molecule upon close approach to the structure are negligible, (b) the atoms within both the gas molecule and nanoparticle have negligible rotational and vibrational energies with respect to translational gas speeds, leading to specular and elastic collisions only, and (c) the long range potential interactions have no bearing on momentum transfer. Instances where these three criteria are met are atypical for structurally complex entities in a diatomic background gas, and instead we propose that the collision cross section in the *PA* method should be calculated as:

$$\Omega = \mathscr{L}\xi PA, \tag{2a}$$

where *PA* is the orientationally averaged projected area, ξ is a dimensionless momentum transfer factor which depends in the manner in which gas molecules impinge upon and are reemitted from the structure, and $\mathscr{L}$ is a dimensionless factor accounting for the influence of long range potential interactions. These two dimensionless factors must be determined either from experimental data (e.g. the Millikan data set suggests that $\xi = 1.36$ [19,20]) or from calculations on model structures. The development of correct *PA* methods provides direct link between the physical dimensions of a structure and the amount of momentum transferred by impinging gas molecules. However, while the incorporation of the correction factors likely leads to a more accurate *PA* method than does their omission, and *PA* calculation itself is not computationally intensive, we note that the decomposition of the collision cross section given by Eq. (2a) is by no means theoretically rigorous, and likely only applies for specific modes gas molecule scattering from surfaces and specific functional forms for the long range potential. For this reason, computations of greater detail need to be performed.

(2) *The diffusive hard sphere scattering (DHSS) method.* The next level of complexity in collision cross section calculation is to perform gas molecule scattering calculations with hard-sphere structures of interest (again with prescribed radii for the base units of the structure and the gas molecule), neglecting any potential interactions between gas molecule and structure. This leads to the determination of the hard-sphere collision cross section Ω_{HS}, from which the full collision cross section is then calculated as:

$$\Omega = \mathscr{L}\Omega_{HS}, \tag{2b}$$

Ω_{HS} calculation with purely specular, elastic collisions is incorporated into MOBCAL's EHSS method [36], with inelastic, non-specular scattering methods considered by others [23,31]. Here, we generalize hard sphere collision cross section calculations, and in the subsequent section we discuss how to perform such calculations for arbitrary structures and

with arbitrary gas molecule scattering laws. As elastic, specular scattering between gas molecules and a structure only apply in the absence of rotational and vibrational energy (when modeling gas molecules as spheres and structures as frozen entities), we term this method the diffusive hard sphere scattering (DHSS) method, distinguishing it from the existing EHSS method.

(3) *Diffusive trajectory method (DTM).* Like Eq. (2a), Eq. (2b) is an approximation which may only apply for particular scattering rules and for particular long range potentials. Therefore, even more rigorous calculation of Ω requires calculation of the momentum transfer to a structure by monitoring the trajectories of oncoming gas molecules in the presence of long range potentials. Following the discussion of the DHSS method, we discuss such trajectory calculations, with the resulting method termed the diffusive trajectory method (DTM).

A comparison of DHSS and DTM predictions with specific gas molecule scattering laws to experimentally measured collision cross sections (for polyethylene glycol and tetralkylammonium ions in air) is given in a related research report [53]. This report specifically examines two non-specular gas molecule scattering rules in the calculations and concludes with an empirical justification for Eq. (2a), and validity of the *PA* method. Although some details on the DHSS and DTM methods are also given, much greater detail on the computation methods is provided here. Further, the performance of these methods in predicting the collision cross sections of model structures, both aggregated ensembles of spheres and fullerenes, is discussed in terms of the number of gas molecule collisions which must be simulated and, in the DTM method, the timestep required for convergence.

2.1.2. Traditional collision cross section calculation techniques

To determine collision cross sections through calculation of the degree of momentum transfer from gas molecules to a structure, one approach, invoked frequently for spheres [10], is the determination of the force ($\delta\vec{P}$) on a small surface element of the structure brought about by the impingement of gas molecules. This force can be calculated using the equation:

$$\delta\vec{P} = -\rho_{gas}\int_{c\cdot n<0}\rho'(\vec{c}'\cdot\vec{n}')\vec{c}'\,d^3c'\delta S, \tag{3}$$

where ρ_{gas} is the mass density of the gas, $\vec{n}$ is the unit outward normal from the surface of the structure, $\vec{c}'$ is the gas molecule velocity vector, and ρ' is the gas molecule velocity vector distribution function. When the gas molecule velocity vector is skewed by a bulk velocity vector $\vec{V}$, integration of the force on each surface element over the entire surface of a structure yields the drag tensor, from which the collision cross section can be extracted. While simple to calculate for each surface element, Eq. (3) conveys two major problems. The first one deals the intrinsic difficulty of integrating over a non-simple, generally non-convex surface. The second problem is specific of concave surfaces, where there will be some inaccessible surface regions which are impenetrable for gas molecules, and others for which parasitic drag, brought about by multiple collisions of the gas molecule, are present.

Therefore, an alternative procedure is invoked in the DHSS and DTM methods, in which it is necessary to (a) select a suitable control volume in which (b) an appropriate sampling of gas molecules can be introduced and where one can (c) monitor gas molecule motion through the control volume, until each examined molecule eventually exits, and (d) relate the change in momentum of entering and exiting gas molecules to the drag force on the structure. These four steps are first discussed for DHSS calculations, with the modifications needed for DTM calculations discussed subsequently.

2.2. Gas molecule velocity distributions

We will express the gas molecule velocity vector distribution function as ρ' in the presence of a bulk flow $\vec{V}$. Assuming the gas molecules are in thermal equilibrium, dimensionlessly the distribution function may be written as:

$$\rho^* = \left(\frac{1}{\pi}\right)^{3/2}\exp(-(\|\vec{c}^* - \vec{V}^*\|^2), \tag{4}$$

where "$*$" denotes in this case dimensionless variables ($\rho' = h^3\rho^*$), normalized using the most probable gas molecule speed $h = \left(\frac{2kT}{m_{gas}}\right)^{1/2}$ (with m_{gas} equal to the mass of a gas molecule).

In cases where the structure of interest is diffusing through the medium, or when mobility measurements are made at low Mach numbers, nonlinear effects can be removed from this distribution via the Chapman–Enskog expansion [29], giving:

$$\rho^* = \frac{1}{\pi^{3/2}}\exp(-(\vec{c}^{*2} + \vec{V}^{*2} - 2\vec{c}^*\cdot\vec{V}^*)) \approx \rho_0^* + 2(\vec{c}^*\cdot\vec{V}^*)\rho_0^* = \rho_0^* + \rho_1^*, \tag{5a}$$

where ρ_0 is the classical Maxwell–Boltzmann velocity distribution:

$$\rho_0 = \left(\frac{m_{gas}}{2\pi kT}\right)^{3/2}\exp\left(-\frac{m_{gas}(c^2)}{2kT}\right). \tag{5b}$$

In Eq. (5a), the distribution function is conveniently separated into two terms. The second term accounts for gas molecule motion in the direction of the bulk velocity, while the first term, the Maxwell–Boltzmann distribution, must impart no

net momentum transfer to the particle as it is exclusively independent of the velocity **V**. Therefore, this first term can be neglected for rectilinear gas molecule trajectories, encountered in DHSS calculations.

2.3. Control volume selection

The goal in control volume selection is to define a domain and corresponding boundary surfaces which completely enclose the structure of interest, and which enable the determination of the net momentum transfer that every gas molecule imparts on the structure while minimizing the need to monitor the trajectories of gas molecules which contribute negligibly to the force on the structure. Of the possible polyhedra that can be used to surround a given object, we opt to use one of two domains for all calculations, either a cuboid or a sphere. The former is used when the structure of interest is appreciably skewed, while the latter is applied to globular objects. To specifically determine the domain shape and dimensions, the minimum length, width, and height for a cuboid and minimum radius for a sphere required to enclose a structure are determined. Of these two, the domain of minimum volume is selected as the control volume.

2.3.1. Cuboid control volume

To perform momentum transfer calculations with a cuboid, it is first necessary to calculate the volumetric flow of gas molecules through each of the cuboid's faces. For this purpose, the bulk velocity is oriented perpendicular to one of the cuboid faces, i.e. $\vec{V} = V\vec{i}$. Because of the neglect of ρ_0 in the gas molecule velocity distribution, negative numerical flows result in some regions of the control surface (e.g. on the face opposing the velocity), as the perturbation distribution ρ_1 is based on a dot product $(\vec{c}\cdot\vec{V})$, which becomes negative every time a particular gas molecule enters the domain against the bulk velocity. This negative flow is physically unreal; in the numerical algorithm the contribution of "negative" gas molecules must be subtracted from the net momentum transfer (i.e. they contribute "negative" momentum). Therefore, positive and negative flows into the control volume must be examined separately so as to not cancel their contributions.

First, considering the front wall, through which the bulk velocity enters, the dimensionless volumetric flowrate Q_{frnt} per unit of dimensionless area (A^*,with A denoting a dimensional area) is given by the equation:

$$\frac{Q_{frnt}}{A^*_{frnt}} = \int_{\mathbf{c}\cdot\mathbf{n}<0} \rho_1^*(\vec{c}^*\cdot\vec{n})d^3c^*, \tag{6}$$

where $\boldsymbol{n}$ is the outwards normal to the control surface and the gas molecules that account for the incoming flow are only those that come into contact with the wall from the outside, leading to $\boldsymbol{c}\cdot\boldsymbol{n} < 0$. Using Cartesian coordinates, with which $c^* = (u^*, v^*, w^*)$:

$$\frac{Q_{frnt}}{A^*_{frnt}} = \frac{1}{\pi^{3/2}}\int_0^\infty\int_{-\infty}^\infty\int_{-\infty}^\infty 2V^*u^{*2}e^{-(u^{*2}+v^{*2}+w^{*2})}du^*dv^*dw^* = V^*/2, \tag{7}$$

where u^* is only positive. Note that Eq. (7) has been solved for using the following integrals:

$$\int_{-\infty}^\infty e^{-x^2}dx = \sqrt{\pi};\quad \int_{-\infty}^\infty x^2e^{-x^2}dx = 1/2\sqrt{\pi};\quad \int_{-\infty}^\infty x^4e^{-x^2}dx = (3/4)\sqrt{\pi};\quad \int_0^\infty xe^{-x^2}dx = 1/2;\quad \int_0^\infty x^3e^{-x^2}dx = 1/2;$$
$$\int_0^\infty x^5e^{-x^2}dx = 1. \tag{8a-f}$$

Conversely, for the back wall, where "negative" gas molecule flow enters:

$$\frac{Q_{back}}{A^*_{back}} = \frac{-1}{\pi^{3/2}}\int_0^\infty\int_{-\infty}^\infty\int_{-\infty}^\infty 2V^*u^{*2}e^{-(u^{*2}+v^{*2}+w^{*2})}du^*dv^*dw^* = -V^*/2, \tag{9}$$

where the subscript "*back*" denotes the back wall. For the side walls, positive (+) and negative (−) flow must be differentiated as:

$$\frac{Q_{side+}}{A^*_{side}} = \frac{1}{\pi^{3/2}}\int_0^\infty\int_0^\infty\int_{-\infty}^\infty 2u^*v^*e^{-(u^{*2}+v^{*2}+w^{*2})}du^*dv^*dw^* = V^*/2\pi; \tag{10}$$

$$\frac{Q_{side-}}{A^*_{side}} = \frac{-1}{\pi^{3/2}}\int_0^\infty\int_0^\infty\int_{-\infty}^\infty 2u^*v^*e^{-(u^{*2}+v^{*2}+w^{*2})}du^*dv^*dw^* = -V^*/2\pi, \tag{11}$$

where (8a-f) have again been used and u varies from $(0,\infty)$ and $(-\infty,0)$ for positive and negative flows, respectively. The total flow through any of the side walls will add up to 0 unless otherwise separated. Following Garcia-Ybarra and Rosner [24] and Mackowski [31], the total number of gas molecules passing through each surface (N) given by the volumetric flowrate and gas molecule number concentration (n), over a period time (t_T) is:

$$N_{frnt} = nhV^*A_{frnt}t_T/2; \tag{12}$$

$$N_{side} = nhV^*A_{sidei}t_T/2\pi + |-nhV^*A_{sidei}t_T/2\pi| = nhV^*A_{sidei}t_T/\pi; \tag{13}$$

Expressing the total number of gas molecules entering the control volume as $N = 2N_{frnt} + 2N_{side1} + 2N_{side2}$, and eliminating t_T from (12) and 13 leads to:

$$N_{frnt} = \frac{NA_{frnt}/2}{A_{frnt} + (2A_{side1} + 2A_{side2})/\pi}; \tag{14}$$

$$N_{sidei} = \frac{NA_{sidei}/\pi}{A_{frnt} + (2A_{side1} + 2A_{side2})/\pi}, \tag{15}$$

where each of the parallel sides (1 and 2) has been considered separately. Similarly, solving for t_T gives:

$$t_T = \frac{2N}{nhV^*(A_{frnt} + (2A_{side1} + 2A_{side2})/\pi)}. \tag{16}$$

Once the volumetric flowrates have been estimated, it is necessary to establish the appropriate thermal speed and angular distributions sampled for gas molecules entering the control volume. For the walls perpendicular to the bulk motion (front and back) these distributions are intrinsically the same, and the position on the surface from which the particles are set in motion will be chosen randomly. In spherical coordinates the emission angles must obey the relationship:

$$\frac{K_1}{\pi^{3/2}} \int_0^{\pi/2} \int_0^{2\pi} \int_0^{\infty} 2V^* c^{*2} \cos^2(\theta) e^{-(c^{*2})} c^{*2} \sin(\theta) d\theta d\phi dc^* = 1, \tag{17}$$

where the inclination angle θ represents the deviation from the positive x direction up to $\pi/2$, and the azimuth angle ϕ varies from 0 to 2π, which permits only those molecules that comply with $\boldsymbol{c} \cdot \boldsymbol{n} < 0$ to be reckoned. Also in Eq. (17), c^* denotes the gas molecule (scalar) speed, and K_1 is a constant set to normalize the left hand side of the equation.

A key benefit to selecting a cuboid for the control volume is that Eq. (17) is separable in c^*, θ, and ϕ. Therefore, not only is it possible to bypass the sampling of the speed, as it is the same for all angles and positions, but also the angles are separable. In DHSS calculations, collision and re-emission rules do not depend on the speed of the colliding gas molecule, and gas molecule trajectories are rectilinear. Hence with DHSS calculations it is possible to simply emit gas molecules into the control volume at their average speed ($\bar{c}_e{}^*$), which is given by the relationship:

$$\bar{c}_e^* = \frac{\int_0^{\infty} 2V^* c^5 e^{-(c^2)} dc}{\int_0^{\infty} 2V^* c^4 e^{-(c^2)} dc} = \frac{8}{3\sqrt{\pi}}. \tag{18}$$

To select a speed from the appropriate distribution (ρ_1) in lieu of using the mean speed, the procedure outlined by Chan and Dahneke [23] may be used. Furthermore, for DHSS calculations, the emission angles can be sampled as follows [31]. First, two uniformly distributed random variables within the range $[0, 1]$, R_1 and R_2, are selected. These random numbers are related to the emission angles through the relationships:

$$R_1 = 3 \int_0^{\theta} \cos^2(\theta) \sin(\theta) \mathrm{d}\theta, \tag{19a}$$

$$R_2 = 1/2\pi \int_0^{\phi} d\phi. \tag{19b}$$

Isolating the angles gives:

$$\cos(\theta) = R_1^{1/3} \quad \text{and} \quad \phi = 2\pi R_2. \tag{19c-d}$$

Similarly, for the walls parallel to the bulk flow, the probability of the distribution can now be written as:

$$\frac{K_1}{\pi^{3/2}} \int_0^{\pi/2} \int_0^{2\pi} \int_0^{\infty} 2V^* c^{*2} \cos^2(\theta) e^{-(c^{*2})} c^{*2} \sin^2(\theta) \cos(\phi) d\theta d\phi dc^* = 1. \tag{20}$$

Here, the angles have been chosen so that $\theta = 0$ defines the vector normal to the wall, and the positive x direction is given by $\theta = \pi/2$ and $\phi = 0$. Again, all variables are separable and the angles can be sampled from:

$$\sin(\theta) = R_3^{1/3} \quad \text{and} \quad \phi = 2R_4 - 1, \tag{21a-b}$$

where R_3 and R_4 are again uniformly distributed random variables on the interval $[0, 1]$.

2.3.2. Spherical control volume

Similar to a cuboidal control volume, the flow of gas molecules through a spherical control volume also needs to be partitioned into gas molecules which transmit positive momentum, and gas molecules which transmit "negative" momentum. However, unlike the cuboid, in which a front wall and a back wall can be clearly defined, the choice of direction for the bulk flow vector for a spherical control volume cannot simplify gas molecule volumetric flow calculations, and "negative" gas

molecules may in fact pass through the control surface at almost any point. The dimensionless positive volumetric flow rate entering the sphere ($sp+$) is given by:

$$Q_{sp+} = -\oint \int_{\boldsymbol{c}\cdot\boldsymbol{n}<0}^{\boldsymbol{V}\cdot\boldsymbol{c}<0} 2\vec{V}^* \cdot \vec{c}^*(\vec{c}^* \cdot \vec{n}) d^3c^* dA^*_{sp}. \tag{22}$$

where dA^*_{sp} is the dimensionless surface element on the sphere. We note that in Eq. (22), only the positive momentum carrying volumetric flowrate is considered ($\boldsymbol{V}\cdot\boldsymbol{c} < 0$), and that the sum of the positive volumetric flowrate and negative volumetric flowrate will always be equivalent over a spherical control surface. Since a sphere is completely symmetric, we opt to leave $\vec{n}$ fixed (i.e. parallel to the x-axis), and correspondingly integrate over all possible positions of $\vec{V}^*$. The positive volumetric flowrate is thus given by:

$$\begin{aligned} Q^*_{sp+} &= \frac{1}{\pi^{3/2}} \int_0^{2\pi}\int_0^{\pi}\int_0^{\infty}\int_0^{2\pi}\int_0^{\frac{\pi}{2}} 2V^* R^{*2}_{sp}[\cos(\chi)\cos(\theta) + \sin(\chi)\cos(\psi)\sin(\theta)\cos(\phi) + \sin(\chi)\sin(\psi)\sin(\theta) \\ &\quad \times \sin(\phi)]\sin(\theta)\cos(\theta)\sin(\chi) c^{*4} e^{-c^{*2}} d\theta d\phi dc^* d\chi d\psi \\ &= (3/4)\pi V^* R^{*2}_{sp}, \end{aligned} \tag{23}$$

where R_{sp} is the radius of the sphere, and the dimensionless sphere radius, R^*_{sp}, is often set to 1. χ and ψ are the inclination and azimuthal angles on the sphere, respectively, both of which are integrated over the entire spherical surface. θ and ϕ are the local angles with respect to the normal and describe the angular position of the velocity vector at position $\boldsymbol{n}$. $\theta = 0$ represents the normal entering direction and is maximally bounded between 0 and $\pi/2$, so as to only consider $\boldsymbol{c}\cdot\boldsymbol{n} < 0$. To compute the integral in Eq. (23), the bounds provided lead to the condition:

$$[\cos(\chi)\cos(\theta) + \sin(\chi)\cos(\psi)\sin(\theta)\cos(\phi) + \sin(\chi)\sin(\psi)\sin(\theta)\sin(\phi)] > 0. \tag{24}$$

The total number of positive momentum gas molecules crossing the control surface is then easily defined using Eq. (23). Also accounting for the volumetric flowrate of "negative" momentum bearing gas molecules with the number of emitted gas molecules as:

$$N = (3/2)\pi n h V^* t_T R^2_{sp} = (3/8) n h V^* t_T A_{wsp}. \tag{25a}$$

where $A_{wsp} = 4\pi R^2_{sp}$ is the wetted surface area of the sphere. The total time t_T required for N gas molecules to cross into the control volume is then determined as:

$$t_T = \frac{8N}{3nhV^* A_{wsp}}. \tag{25b}$$

Finally, to examine momentum transfer from incoming gas molecules, it is necessary define gas molecule initial positions and trajectories. In DHSS calculations, Eq. (18) may be similarly used for the speed of all incoming gas molecules into a spherical control volume, as can the Chan and Dahneke [23] sampling scheme when a distribution of speeds in required. However, the angles defining the trajectory initially must be different through a different manner, as they are not separate from one another, and further depend upon position on the control surface (χ and ψ). A reasonably simple method to determine χ, ψ, θ and ϕ, is to choose random values for all 4 angles within their given domains and check if they comply with the criteria in Eqs. (23) and (24). If the chosen angles do not, then a new set of random selected angles must be selected, and the process repeats until a suitable combination is found.

2.4. Collision and reemission rules

Once the control volume and the corresponding initial positions and velocity vectors of gas molecules have been defined, the trajectories, impingement, and reemission of gas molecules can be analyzed. Given the direction of an entering gas molecule, we immediately determine if the collision between gas molecule and the structure will occur using the following procedure: A gas molecule entering the control volume at position x_0 with unit velocity direction vector v_0 has a perpendicular distance, D, from an atom/base unit of the structure with its center of mass at $\boldsymbol{c}_m$:

$$D = |(\vec{c}_m - \vec{x}_0) - ((\vec{c}_m - \vec{x}_0)\cdot\vec{v}_0)\vec{v}_0|. \tag{26}$$

If D is less than the sum (R) of the gas molecule radius and the atom/base unit radius (both modeled as spheres) then the gas molecule would collide with the atom/base unit in question, with the collision point x_s defined as:

$$\vec{x}_s = \vec{x}_0 + \left((\vec{c}_m - \vec{x}_0)\cdot\vec{v}_0 - \sqrt{R^2 - D^2}\right)\vec{v}_0. \tag{27}$$

If a collision is detected, an event is counted, and the collision point is determined from the minimum distance the gas molecule must travel to collide with the structure (as D may be less than sum of the gas molecule radius and the atom/base unit radius for multiple atoms/base units). Correspondingly, the outward normal vector from the collision point, $\mathbf{n}_{out}$, is calculated as:

$$\vec{n}_{out} = \vec{x}_s - \vec{c}_m \,. \tag{28}$$

Identification of the collision point permits calculation of the reemission trajectory. Ideally, this would be accomplished through molecular dynamic modeling of not only gas molecules, but also the atoms within a structure. However, this approach is presently computationally too expensive to employ for structures composed of more than a handful of atoms, and with the use of rigid structural models, a specific, semi-empirical reemission model is required. As noted in the introduction section, several different reemission laws are available in the literature, including a specular reemission rule with conservation of gas molecule translational energy (elastic scattering), and various forms of diffuse reemission, with random reemission angles and thermal accommodation of the gas molecule relative to the internal energy of the structure it collides with [10].

Although the specular, elastic reemission law alone is invoked in MOBCAL algorithms, this is not in line with experimental measurements in diatomic gases. A succinct derivation [53] reveals that when the analytic derivation of Eq. (1) is compared with experimental measurements of 1.5–10 nm spherical particles [12,14,19,20,54], Ω is equivalent to 1.36PA. The specular, elastic reemission rule cannot reproduce this result for realistically sized gas molecules (the specular model yields $\Omega = PA$ for a smooth sphere), and with this failure of specular models, alternative, diffuse reemission rules need to be input into DHSS and DTM algorithms. However, the precise reemission rules which lead to experimental observations are presently unclear [55], and future work is necessary to elucidate the physics of such collisions. A commonly invoked explanation of experimental observations is that of Epstein [10], who proposed a number of specular and diffuse reemission rules. In the most prominent of these diffuse rules, gas molecules are reemitted at a random angle from the surface of a structure, with the reemission speed sampled from a Maxwell–Boltzmann distribution at the temperature of the surface (complete thermal accommodation). When applied to a sphere, this rule, attempting to mimic instant exchange between atomic vibrational and rotational energy from both the gas molecule and the structure with gas molecule translational energy, yields $\Omega = (1+\pi/8)PA \approx 1.39PA$. To better match experimental results, Epstein, with Millikan, introduced an "accommodation coefficient" α, which is the fraction of impinging gas molecules which obey Epstein's diffuse reemission rule, with the remaining $1-\alpha$ colliding specularly and elastically with a structure. $\alpha = 0.91$ leads to good agreement with most experimental results. Epstein also proposed a second diffuse reemission rule, in which gas molecules are reemitted at a random angle, but retain their translational energy. Applying this rule to a sphere yields $\Omega = (1+9\pi/64)PA \approx 1.44PA$, and would require an accommodation coefficient of 0.81 to match experimental data. Based on the existing precedent of invoking these reemission rules, in the present work we also invoke Epstein's diffuse reemission rules as well as the specular reemission rule to be used in DHSS and DTM calculations, with an input accommodation coefficient defining the fraction of gas molecule collisions which obey the prescribed diffuse reemission rule (either with complete thermal accommodation or with conserved translational energy). We do note, however, that the algorithms provided here can be modified to handle alternative reemission rules, and that reemission rules can be proposed which agree with experimental results without the use of an accommodation coefficient [53].

For the diffusely reemitted gas molecules with complete thermal accommodation, the dimensionless reemitted speed (c_r^*) from the collision point can be determined from the equation:

$$\frac{K_1}{\pi^{3/2}} \int_0^{\theta} \int_0^{\phi} \int_0^{c} c_r^{*3} e^{-(c_r^{*2})} \cos(\theta)\sin(\theta) d\theta d\phi dc_r^* = R_5, \tag{29}$$

where R_5 is a uniformly distributed random variable on the interval $[0,1]$ and K_1 retains its definition from Eq. (17). Note that if the structure is at a different specified temperature than the surrounding gas (i.e. thermal equilibrium is not established between gas molecule and the structure), then the dimensionless reemitted speed distribution in Eq. (29) must be adjusted accordingly to reflect this temperature difference. Like Eqs. (17) and (20), all variables are separable in Eq. (29), and with rectilinear trajectories in DHSS calculations, the speed of all reemitted gas molecules can be determined as the mean reemission speed, $\bar{c}_r^*$:

$$\bar{c}_r^* = \frac{\int_0^{\infty} 2V^* c^{*4} e^{-(c^{*2})} dc^*}{\int_0^{\infty} 2V^* c^{*3} e^{-(c^{*2})} dc^*} = \frac{3\sqrt{\pi}}{4}, \tag{30}$$

which differs from the mean speed for gas molecules entering the control surface. The reemission angles for diffuse reemission are calculated as:

$$\cos(\theta) = R_6^{1/2} \quad \text{and} \quad \phi = 2\pi R_7. \tag{31a-b}$$

where R_6 and R_7 are again defined as uniformly distributed random variables on $[0,1]$. For gas molecules that collide specularly, the unit direction vector of reemission ($\vec{v}_r$) is calculated deterministically as:

$$\vec{v}_r = \vec{v}_0 - 2(\vec{v}_0 \cdot \vec{n})\,\vec{n}\,. \tag{32}$$

Each time an emitted gas molecule collides with a structure, a uniform random variable on $[0,1]$ is calculated. If this value is less than the prescribed value of α, diffusive reemission rules are followed; otherwise, specular rules are used. Following reemission, the collision check is again performed, and in the event of a subsequent collision, a new random number is calculated and the reemission speed and direction are again determined using the selected reemission rule. This process is repeated for each emitted gas molecule until they leave the control volume through the control surface.

2.5. Collision cross section determination

After N gas molecules have been introduced into the control volume, requiring a total time t_T (Eq. (16) or (25b)), the drag force on the structure when placed in a specific orientation relative to the oncoming flow, $\vec{F}_D$, is given by the relationship:

$$\vec{F}_D = -\frac{hm_{gas}}{t_T}(\bar{c}_e^*\,\vec{I} + \bar{c}_r^*\,\vec{I}_r) * sign(\vec{V}\cdot\vec{u}), \tag{33a}$$

where:

$$\vec{I} = \sum_{i=1}^{M}\hat{\vec{v}}_0 \quad \text{and} \quad \vec{I}_r = \sum_{i=1}^{M}\hat{\vec{v}}_r, \tag{33b-c}$$

where M is the total number of collision events per N emitted gas molecules, $\hat{\vec{v}}_0$ and $\hat{\vec{v}}_r$ are the incoming and reemitted unit velocity vectors, and $sign(\vec{V}\cdot\vec{u})$ distinguishes positive momentum from negative momentum bearing gas molecules. When t_T is substituted for accordingly, it becomes clear that the drag force is linearly related to the bulk velocity, which is specifically due to the linearization of the gas molecule velocity distribution function (and hence only applies at low speeds relative to the mean thermal speed). Further, the collision cross section also does not vary with bulk velocity in this limit in the absence of potential interactions. Supposing that all orientations of the structure relative to the bulk flow are equally probable, a drag tensor [**B**] can be constructed by calculating the drag force produced by the bulk flow in three perpendicular directions, leaving the dimensionless drag tensor with terms evaluated as:

$$B_{ij} = I_{ij} + \bar{c}_r^*/\bar{c}_e^* I_{r_{ij}}. \tag{34}$$

This drag tensor, irrespective of the structure of interest, is symmetric and positive definite, provided that no rotation is imparted on the structure. As demonstrated by Happel and Brenner [56], such a drag tensor can be diagonalized, and following diagonalization the orientationally averaged collision cross section can be calculated as:

$$\Omega = \frac{3}{nht_T}\left(\frac{1}{B_{11}} + \frac{1}{B_{22}} + \frac{1}{B_{33}}\right)^{-1} \tag{35a}$$

and thus the mobility measured is:

$$Z_p = \left(1 + \frac{m_{gas}}{m_w}\right)^{1/2}\frac{3\sqrt{\pi}ze}{8nhm_{gas}\Omega}, \tag{35b}$$

where B_{ii} denotes the principal values of the drag tensor and m_w is the molecular weight of the ion (the mass factor in Eq. (35b) $\left(1+\frac{m_{gas}}{m_w}\right)^{1/2}$ is necessary to correct for the inertial mass that appears in a regular two body problem). We note further that orientation weighted collision cross sections could also be determined from the described approach; whether or not nanometer scale ions are aligned preferentially during mobility measurements will need to be determined in future work for commonly employed measurement conditions.

2.6. Modifications for the diffuse trajectory method

Several significant changes must be made to the presented method to incorporate the influence of potential interactions on collisions. Overwhelmingly, for charged nanoparticles and ions migrating through non-monoatomic gases, the ion-induced dipole (polarization) potential has the strongest influence on collision dynamics. Therefore, we consider only this interaction potential here. Shorter range Lennard–Jones forces may also be included in calculations, though at a substantial cost of computation speed. Further, we contend that with appropriately sized atoms/base units in a structure at the temperature in question, hard sphere model predictions will agree reasonably well with predictions incorporating Lennard–Jones potentials.

For singly charged, spherical entities, the polarization potential becomes significant at diameters smaller than approximately 1.4 nm in air or molecular nitrogen background gas, and at larger sizes in stronger polarizability gases such as carbon dioxide. The polarization energy, U_{pol}, for a gas molecule which is a distance r_i from a net charge ze, is given by [32]:

$$U_{pol} = -\frac{\alpha_{pol}z^2e^2}{8\pi\varepsilon\varepsilon_0 r_i^4}, \tag{36}$$

where α_{pol} is the polarizability of the background gas molecules ($\sim$1.7 Å^3 for air, N_2, and O_2), ε_0 is the permittivity of free space, and ε is the background gas dielectric constant. The first major change to the computation method necessary to incorporate the influence of this potential is the modification of the gas molecular velocity distribution function; since the trajectory each gas molecule takes in the presence of a potential is dependent on its initial velocity, the initial velocity distribution must be defined completely. Therefore, rigorously, the influence of the Maxwell–Boltzmann term, ρ_0 in Eq. (5) cannot be neglected (though the possibility of its exclusion is examined in the results and discussion section of this work). This point is overlooked in MOBCAL's trajectory method [13], and ρ_0 is neglected when potentials are included in this calculation which

may affect results for charged structures of similar sizes to gas molecules themselves. Including ρ_0 in the gas molecule velocity distribution function, however, drastically increases computation time, and we hence consider simplifying this distribution without a significant loss in precision.

All DTM calculations are performed using a cuboid control volume, and with the inclusion of the full gas molecule velocity distribution, the dimensionless volumetric flowrate per area through the front $(f,+)$ and back $(b,-)$ walls is calculated as:

$$\frac{Q_{fb\pm}}{A^*_{fb}} = \frac{1}{\pi^{3/2}} \int_0^{\pi/2} \int_0^{2\pi} \int_0^{\infty} (1 \pm 2V^* c^* \cos(\theta)) e^{-(c^{*2})} c^{*3} \cos(\theta) \sin(\theta) dc^* d\theta d\phi = \frac{1}{4\sqrt{\pi}} \pm V^*; \tag{37}$$

$$\frac{Q_{side\pm}}{A^*_{side}} = \frac{1}{\pi^{3/2}} \int_0^{\pi/2} \int_0^{2\pi} \int_0^{\infty} (1 \pm 2V^* c^* \cos(\phi) \sin(\theta)) e^{-(c^{*2})} c^{*3} \cos(\theta) \sin(\theta) dc^* d\theta d\phi = \frac{1}{2\pi^{3/2}} \pm V^*. \tag{38}$$

In Eq. (37) the + and − correspond to the front and back walls respectively, while in Eq. (38) + and − correspond to the gas molecule flow aligned with the bulk flow or opposing the bulk flow, respectively. With the total number of emitted gas molecules, N, the number of gas molecules introduced on the front and back walls (N_{fbT}) is expressed as:

$$N_{fbT} = \frac{N}{1 + \frac{A_{sideT}}{A_{fbT}}} \tag{39a}$$

and correspondingly the total number introduced to side walls (N_{sideT}) is expressed as:

$$N_{sideT} = N_{fbT} \frac{A_{sideT}}{A_{fbT}} \tag{39b}$$

where the subscript "T" denotes the sum (of the number or the area) of the front and back wall or all side wall contributions. The total time taken for these molecules to pass through the control volume is determined as:

$$t_T = \frac{\sqrt{\pi} N_{fbT}}{nhA_{fbT}} \tag{40}$$

Similarly, in the DTM method the distributions from which to select the gas molecule initial speeds (note that in this case the mean speed may not be used for all gas molecules) are expressed as:

$$d\rho^*_{fb} = K_4 e^{-c^{*2}} \vec{c}^* \cdot \vec{n} (1 - 2\vec{V}^* \cdot \vec{c}^*) d^3 c^* = \frac{4}{1 \pm \sqrt{\pi} V^*} (1 \pm 2V^* c^* \cos(\theta)) e^{-c^{*2}} c^{*3} \sin(\theta) \cos(\theta) d\theta d\phi dc^* \tag{41a}$$

for the front and back walls, and for the side walls:

$$d\rho^*_{side} = K_5 e^{-c^{*2}} \vec{c}^* \cdot \vec{n} (1 - 2\vec{V}^* \cdot \vec{c}^*) d^3 c^* = \frac{4}{\pi \pm 2\sqrt{\pi} V^*} (1 \pm 2V^* c^* \sin(\theta) \cos(\phi)) e^{-c^{*2}} c^{*3} \sin(\theta) \cos(\theta) d\theta d\phi dc^*, \tag{41b}$$

where the $\pm$ sign has the usual connotation. Emission speeds and angles are selected via the equation:

$$\int d\rho^*_{fb,side} = R_8 \tag{41c}$$

in an analogous fashion to speed and angle selection in Eq. (29).

The second major change necessary for DTM calculations is that gas molecule trajectories are no longer rectilinear. To allow for the initial velocity vectors to be selected with Eqs. (41a)–(41c), on the control surface, the potential energy to thermal energy ratio, Ψ:

$$\Psi = \frac{PE}{KE} = \frac{\alpha_{pol} z^2 e^2}{12\pi\varepsilon_0 k T r_0^4}, \tag{42}$$

must be sufficiently low. In air or molecular nitrogen at 304 K with a singly charged entity, the radius r_0 at which $\Psi = 0.005$ is 15.9 Å, thus in addition to enclosing the structure of interest, the control surface is at least 15.9 Å from any charge located on the structure. This distance is adjusted accordingly when 2 or more charges are in the system, so as to ensure that Ψ is kept at 0.5%.

To then calculate gas molecule trajectories through the control volume, a modified velocity-Verlet algorithm is employed. This algorithm, and other alternatives, are discussed in detail elsewhere [57]. The timestep utilized in calculations is chosen in an effort minimize CPU cost, with the dimensional timestep, Δt, chosen as:

$$\Delta t = \min\left[\beta_1 \frac{r_c^2}{z^2}, \beta_2 r_a^2\right], \tag{43}$$

where β_1 and β_2 are input parameters, r_c and r_a are the distances to the closest charged point or neutral atom, respectively, and z is the number of elemental charges at distance r_c. In the calculations performed to date, the values of β_1 and β_2 have been chosen so that the timestep varies normally between 10^{-14} and 10^{-16} s for molecular nitrogen gas at atmospheric

pressure and 304 K, where larger timesteps are employed at greater distances from the structure. Overall, this method allows for efficient calculation of trajectories, such that DTM computations can be performed on modern desktop and laptop computers, requiring <24 h of time for structures composed of thousands of atoms. While the trajectories are being calculated, we make use of an optimized collision detector that allows calculation of the impact position on the structure. Once the collision has been detected, a bisection method calculates the impaction point on the structure with a .001% error.

The third set of changes needed for DTM calculations focus on the reemission rules. As in DHSS calculations, colliding gas molecules are reemitted either by a diffuse rule or the specular rule, with an input accommodation coefficient determining the fraction of gas molecules obeying each rule. However, when invoking the diffuse reemission rule with thermal accommodation, rather than simply reemitting gas molecules at a mean speed (Eq. (30)), the speed distribution (Eq. (29)) is sampled to determine each reemission speed, and the increase in kinetic energy that the gas molecule received as it moved from the initial point on the control surface to the contact point (because we consider attractive potentials, the kinetic energy is always higher at contact) is added to the sampled reemission speed as:

$$c_r = \left(c_M^2 + \frac{2\sum U_{pol}(\vec{x}_s - \vec{x}_i)}{m_{gas}} \right)^{1/2}, \tag{44}$$

where c_M is the Maxwell speed calculated from the distribution, x_i is the position of the charges and x_s the reemission point. The use of a sampled speed from a distribution, rather than the use of the mean speed, is necessary as it allows the method to account for the influence of gas molecules reemitted at low speeds, which may be drawn back towards the structure for subsequent collisions by the polarization potential. The addition of the gained kinetic energy by the gas molecule into the reemission ensures conservation of energy applies to the examined system.

As a final note on adjustments made for DTM calculations, in the presence of potential interactions, all gas molecules will have their momentum altered as they pass through the control volume, independent of whether they directly collide with the structure. Therefore, in Eqs. (33a)–(33c), the number of collision events M and the number of sampled gas molecules N are exactly equal in DTM calculations. Instances in which gas molecules transfer momentum to a structure without direct collision are referred to as "grazing" collisions, and are addressed in Section 3.

3. Results and discussion

3.1. Example calculation conditions

The DHSS and DTM methods are evaluated in terms of the number of gas molecules trajectories which must be monitored for convergence to the calculated collision cross section, considering both diffuse and specular reemission rules. The sensitivity of DTM calculations to timestep is also investigated. DTM calculations are further performed under specific dimensional conditions, at atmospheric pressure, a temperature of 304 K in molecular nitrogen gas (with gas molecules modeled as spheres with a radii of 1.5, a value based on experimental measurements of the physical dimensions of the N_2 molecule [58]), with a bulk speed of 40 m/s (a typical speed for charged, nanoscale entities in linear mobility spectrometers [2,18], and well below the mean thermal speed).

DHSS calculations are first examined for a smooth sphere, and subsequently for ensembles of spheres as point-contacting quasifractal aggregates, which approximately obey the relationship $N_{prim} = k_f (R_g/a_{prim})^{Df}$, where N_{prim} is the number of base unit spheres in the aggregate, k_f is a dimensionless pre-exponential factor (set to 1.3 for all calculations), R_g is the aggregate radius of gyration, a_{prim} is the base unit radius, and D_f is the fractal dimension, ranging from 1.0 for a perfect straight chain to 3.0 for a densely packed structure. Soot nanoparticles frequently adopt this morphology [59], as do many inorganic nanoparticles synthesized in high temperature reactors [60], hence the transport and reactivity of such particles are of considerable interest [48,49,51,61]. Random quasifractal aggregates, satisfying the noted relationship with a prescribed N_{prim} and D_f are generated using a cluster–cluster aggregation method as is described by Filippov et al. [62]. With such aggregates and prescribed gas molecule reemission rules, the validity of Eq. (2a) with $\mathscr{L} = 1$ is examined, i.e. whether a constant ξ can link the collision cross section and orientationally averaged projected area for varying shapes and modes of gas molecule-structure collisions under hard sphere conditions is determined. Similar DHSS calculations are also reported for symmetric, isotropic structures akin to fullerenes. The presented DTM calculations focus on the collision cross section for a singly charged nanoscale sphere with an N_2 sized gas molecule, but under specular conditions. The focus of such collisions is to examine the parameter $\mathscr{L}$ for this simplified case (where $\xi = 1$) with additional efforts made to isolate the influence of grazing collisions from true gas molecule-structure contact collisions and to study the influence of simplifying the gas molecule velocity distribution function on calculation results.

3.2. DHSS calculations

3.2.1. Spherical structure calculations

Calculations of the collision cross section of a sphere are performed considering 100% specular-elastic collisions (case 1), 100% diffuse collisions with thermal accommodation (case 2), and 100% diffuse collisions without thermal accommodation

(case 3) with a varying number of gas molecule trajectories monitored. The average value of $\xi = \Omega/PA$ over 200 separate calculations is shown as a function of the number of gas molecules used in each calculation (in each orientation, with 3 orientations examined) in Fig. 1(a). Immediately apparent is that for all three invoked reemission rules, calculations converge to the values of ξ found analytically by Epstein [10], demonstrating the correctness of DHSS calculation collision cross sections. Further, for all three remission rules, DHSS calculations are found to converge to the collision cross section rather quickly; after approximately 1000 gas molecule trajectories the RSD is ~0.02.

3.2.2. Quasifractal aggregate structure calculations

For specular elastic collisions with an infinitesimal gas molecule, Fig. 1(b) displays the values of $\xi = \Omega/PA$ for two specific quasifractal aggregates, one dense ($k_f = 1.3$, $D_f = 2.4$, $N_{prim} = 180$, results denoted with open circles) and the other reasonably open ($k_f = 1.3$, $D_f = 1.5$, $N_{prim} = 200$, results denoted with open circles), as functions of the number of gas molecule trajectories examined per orientation. Depictions of the aggregates are displayed on the figure. Also shown are the RSDs for $\xi = \Omega/PA$ (dense aggregate-short dashed line, open aggregate-solid line) as functions of N; these functions differ from one another due to the different void volumes inside the control volumes used to analyze these structures (the sphere for the dense aggregate, and the cuboid for the open aggregate). By instead plotting the RSDs as functions of M, the number

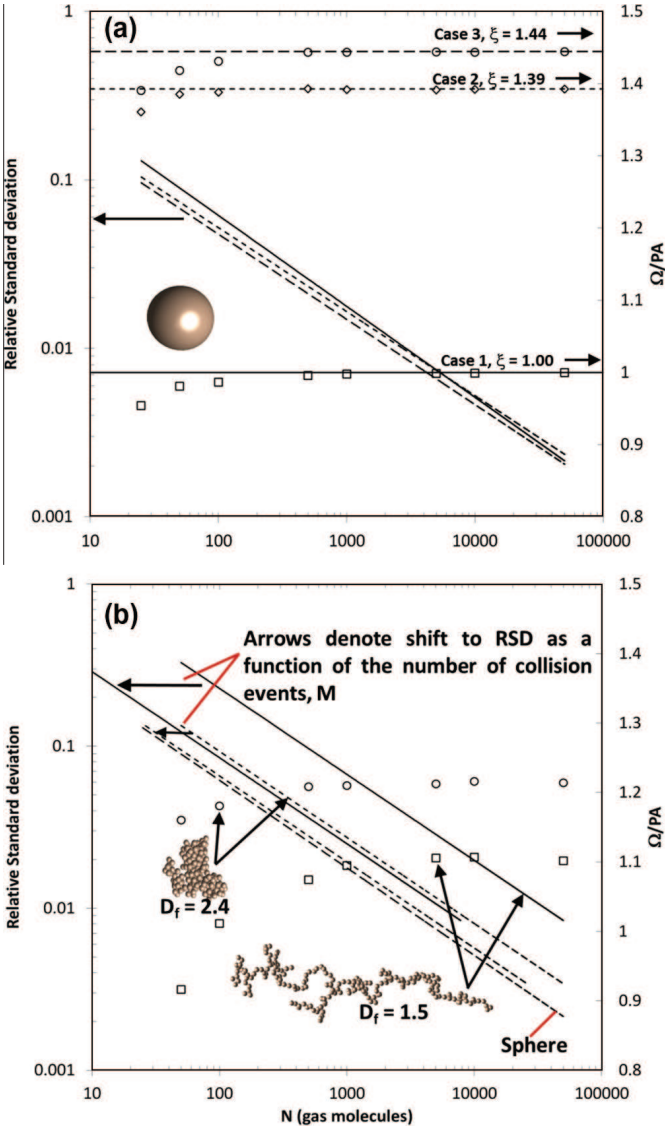

Fig. 1. (a) The relative standard deviation and Ω/PA values obtained for DHSS calculations on a sphere with an infinitesimal gas molecule as a function of the number of simulated trajectories using specular remission rules (case 1), diffuse reemission rules with thermal accommodation (case 2), and diffuse reemission rules with translational energy accommodation (case 3). (b) The relative standard deviation and Ω/PA values obtained for DHSS calculations on quasifractal aggregates under specular elastic conditions identical to (a) case 1. RSD values shown as functions of both the number of trajectories simulated and the number of collision events.

of collision events, as is additionally shown, is brought in better agreement with the results for a sphere. However, the resulting values of $\xi = \Omega/PA$ which calculations converge to are distinct from the value of 1.00 found for a sphere, with ξ approaching 1.21 for the dense aggregate and 1.1 for the open aggregate. This increase in ξ is brought about solely by a fraction of the gas molecules which enter the control volume and collide with the structure in multiple instances prior to exiting, as the angle at which such gas molecules leave the control volume relative to the entrance trajectory does not exactly depend on the manner in which they first collided with the structure, akin to diffuse reemission.

Multiple collisions with specular reemission rules are hence studied for multiple types of quasifractal aggregates, with results shown in Fig. 2(a) and (b). Specifically, Fig. 2(a) shows $\xi = \Omega/PA$ as a function of N_{prim} for $k_f = 1.3$, and $D_f = 1.5$, 1.8, 2.1, and 2.4 (with each result point representing calculations for a single structure satisfying the noted fractal relationship). Best fit curves (linear in Ω/PA versus $\log[N_{prim}]$) are provided for guidance, and depictions of typical structures with these fractal parameters are also displayed on the figure. 100,000 gas molecule trajectories are utilized to obtain the displayed results, which again are for infinitesimal gas molecules. Fig. 2(b) similarly plots $\xi = \Omega/PA$ for these aggregates, but with a gas molecule radius equivalent to the base unit sphere radius. In all cases Ω/PA increases with increasing N_{prim}, with higher values found for higher fractal dimension structures and with finite sized gas molecules. This suggests that for specular reemission, Eq. (2a) cannot be applied, as ξ is not independent of the morphology of the structure under examination, nor the gas molecule size. However, for no tested quasifractal aggregate does Ω/PA approach the experimentally inferred

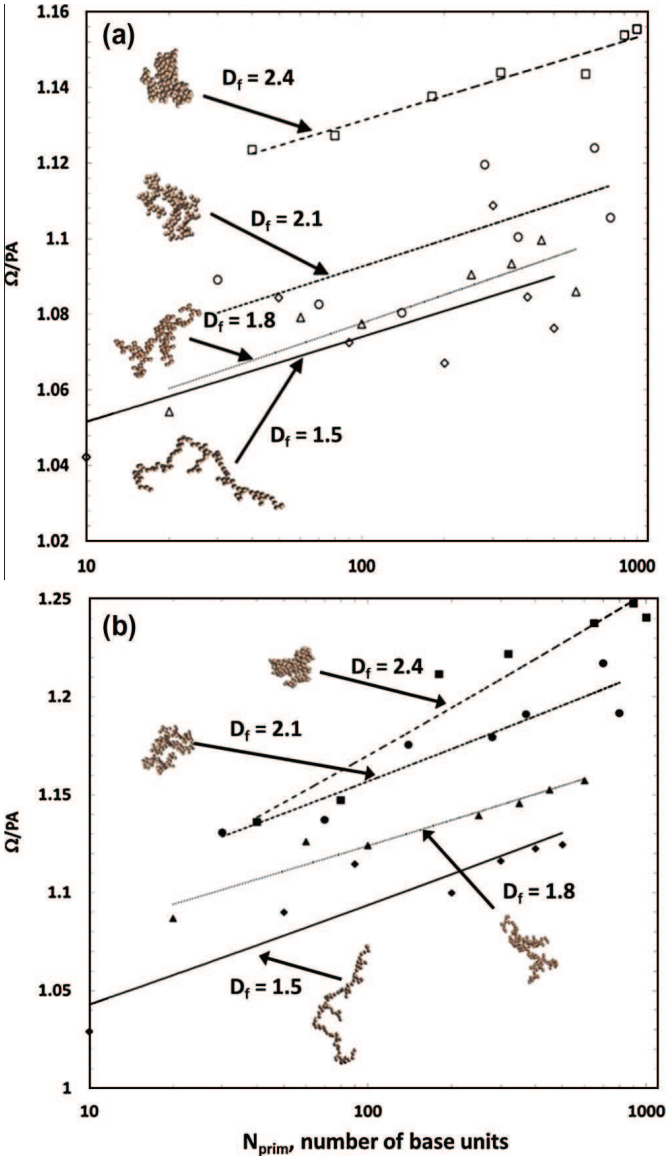

Fig. 2. (a) Variation in Ω/PA values with the number of base units per structure obtained for DHSS calculations on quasifractal aggregates with infinitesimal gas molecules and specular reemission rules. (b) Similar calculation results with gas molecules with radii equivalent to the base sphere radii.

value for diatomic gases, and it is known that dense structures of less than 1000 atoms (1000 base units) still lead to $\xi = 1.36$ [20], which again emphasizes that the specular reemission rule cannot explain experimental results.

Conversely, as evidenced in Fig. 3 (a plot of $\xi = \Omega/PA$ as a function of N_{prim} for $k_f = 1.3$, $D_f = 1.5, 2.4$ aggregates, with diffuse and thermal accommodating as well as diffuse but translational energy conserving reemission rules), when utilizing both diffuse reemission rules, ξ differs ~2% across the entire N_{prim} range examined, with only a weak dependence on D_f found. Further, the radius of the gas molecule does not appear to substantially influence these calculations, suggesting that for diffuse reemission rules, it is possible to define a value ξ for implementation in Eq. (2a) which is nearly independent of the structure of the entity under examination, as well as the gas molecule size (results not shown).

3.2.3. Fullerene structure calculations

All examined quasifractal aggregates contain point contacts between base units, which differs from structures modeling covalently bonded macromolecular ions. We thus elect to examine the collision cross sections of 10 fullerene-like structures composed of 20, 40, 60, 70, 100, 180, 240, 500, 540 and 720 identical base units, respectively. Each base unit has a radius of 1.7, matching the van der Waals radius of carbon (1.7 Å). Collision cross sections for these structures are calculated using the specular reemission rule with gas molecule radii of 0, 1.0, and 1.5, and using both diffuse scattering methods with a gas molecule radius of 1.5. The resulting Ω/PA for all calculations are shown in Fig. 4, along with depictions of the fullerene structures. As with the quasifractal aggregates, specular reemission rules are a function of the number of base units in fullerene structures. However, unlike results found with quasifractal aggregates, the ratio $\xi = \Omega/PA$ decreases with increasing gas molecule radius. This is apparently brought about by the inability of larger gas molecules to access the interstitial regions of the fullerene structures, limiting their ability to collide multiple times with the surface. In spite of this difference in behavior, the specular scattering Ω/PA value is still found to be substantially different than is found in non-monoatomic background gas measurements, and could only approach experimental values for an extremely rough fullerene surface (large N_{prim}) and with gas molecules which are negligibly small compared to the base units. Conversely, both diffuse reemission rules again lead to seemingly invariant values of ξ, which converge to the values Epstein calculated for a sphere.

3.3. DTM calculations

3.3.1. Relative standard deviation and fixed time step

A plot of the RSD determined using 20 DTM calculations as a function of the number of gas molecule trajectories monitored for a 4.0 radius spherical structure in N_2 background gas with elastic specular reemission rules is shown in Fig. 5. The convergence rate is much slower than in the DHSS method; in this instance at least 3 million gas molecule trajectories must be monitored to reach a RSD of 0.02. The large increase in the number of gas molecule trajectories which must be monitored is brought about by the increased control volume requirements of the polarization potential as well as on the addition of the

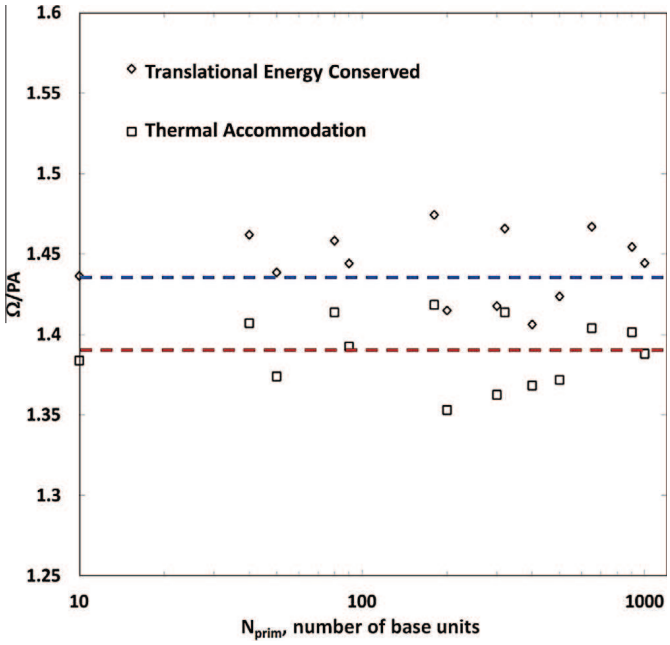

Fig. 3. Variation in Ω/PA values with the number of base units per structure obtained for DHSS calculations on quasifractal aggregates with infinitesimal gas molecules and diffuse reemission rules. Only results for aggregates with fractal dimensions of 1.5 and 2.4 are shown, and are not distinguished from one another.

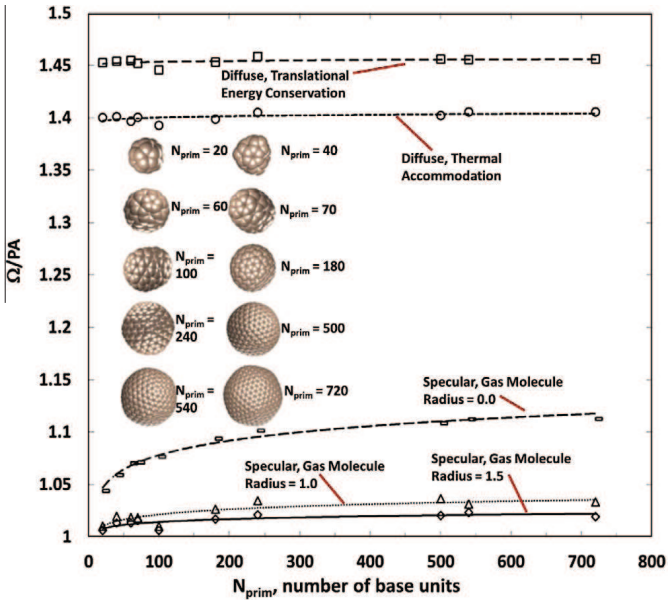

Fig. 4. Variation in Ω/PA values with the number of base units per fullerene structure in DHSS calculations using various reemission rules and gas molecule radii.

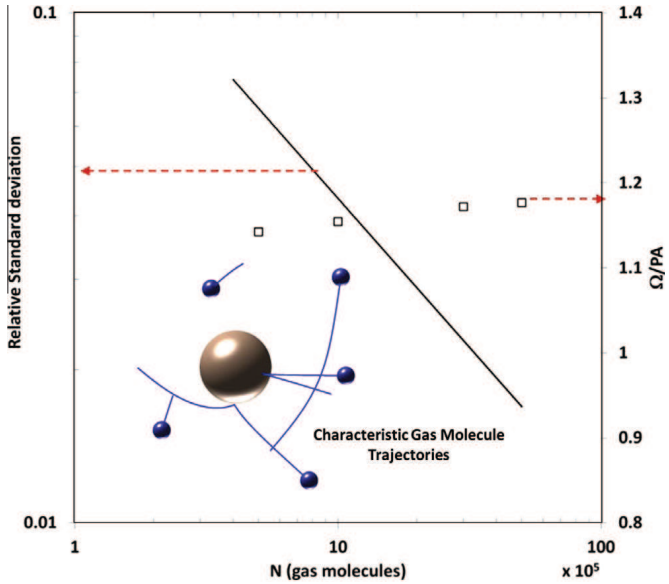

Fig. 5. The relative standard deviation and Ω/PA values for a 4 Å radius sphere in N_2 background gas at 304 K for DTM calculations at atmospheric pressure and 304 K.

main distribution ρ_0 (Eq. (5b)). Most of the gas molecules emitted into the control volume exit without direct collision, yet they still contribute to the structure's collision cross section. Also in Fig. 5, the ratio Ω/PA is plotted on the right side y-axis. Due to polarization, Ω/PA approaches 1.17 for this spherical particle, and given that $\xi = 1.00$ for a sphere with the specular reemission rule, this result suggests $\mathscr{L} = 1.17$ for these conditions.

The influence of (fixed) timestep on the calculation result is examined in Fig. 6, which is a plot of the normalized computing time required to monitor 3 million trajectories, as well as Ω/PA variation with timestep for the same conditions noted for Fig. 5. The timestep is varied in the range 5×10^{-14} to 1×10^{-16} s, and 1 computing time unit is taken as the time required to complete calculations with a timestep of 5×10^{-14} s (approximately 200 s on a 1.6 GHz single core). While little variance in Ω/PA is observed in the examined range, for smaller or more highly charged structures, smaller timesteps may still be necessary; though these results suggest that timesteps on the larger end of the range examined here may be used for larger singly charged structures.

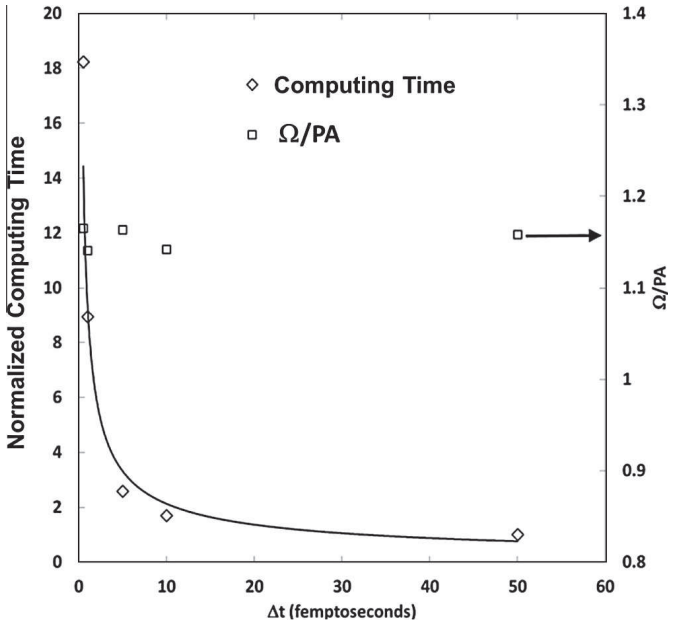

Fig. 6. The normalized computing time required to complete DTM calculations under the conditions noted in Fig. 5 as a function of timestep. Ω/PA variation with timestep is also shown.

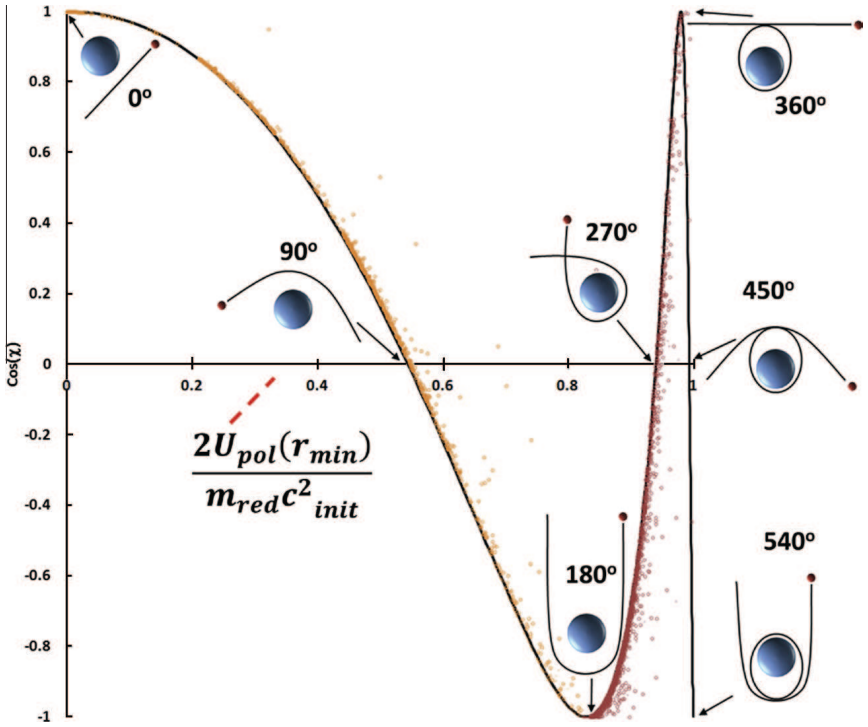

Fig. 7. The cosine of the deflection angle for grazing collisions with a singly charged structure as a function of the polarization energy at half the gas molecule impact parameter normalized by its incoming kinetic energy.

3.3.2. Grazing collisions with singly charged spheres

Initial DTM calculations indicate the influence of grazing collisions on the collision cross section is significant, yet assessment of grazing gas molecule influence is computationally expensive relative to the influence of direct collisions. We therefore attempt to isolate the contributions of grazing collisions, by examining analytically the collision of an infinitesimal gas molecule with a point charge. Following Kennard [63], one can arrive at a simple differential equation that allows us to calculate the complete trajectory:

$$\frac{C_{init}^2}{2} - \frac{\dot{r}^2}{2} = \frac{\gamma^2}{2r^2} - \frac{1}{m_{red}} \int_r^\infty F(r)dr, \tag{45}$$

where C_{init} is the gas velocity at infinity, r is the polar distance centered on the charge, F is the central force and γ is the angular momentum constant. In the case of an attractive force of the type A/r^5, the only solution known is a rather complicated Jacobi elliptic function with double periodicity [64] where, in the absence of a much needed focused study, other means must be used to extract information. Nonetheless, as shown elsewhere [65–67], conservation of energy, linear momentum, and angular momentum leads to a relationship between the gas molecule's initial impact parameter (b, the initial radial distance between the gas molecule and the point massand $\gamma = bC_{init}$), the minimum radial distance the gas molecule will reach from the point charge (r_{min}), and the radially varying potential interaction (U) experienced by the gas molecule:

$$b^2 = r_{min}^2 \left[1 + \frac{2}{c_{init}^2 m_{red}} \int_{r_{min}}^\infty F(r)dr \right] = r_{min}^2 \left[1 + \frac{2U(r_{min})}{c_{init}^2 m_{red}} \right]. \tag{46}$$

For the polarization potential, it is found with Eq. (46) that in instances where $b^4 < \alpha_{pol} z^2 e^2 / (\pi \varepsilon \varepsilon_0 C_{init}^2 m_{red})$ a real apside r_{min} cannot exist; i.e. the gas molecule collides directly with the center of the point charge for these conditions. Therefore, irrespective of

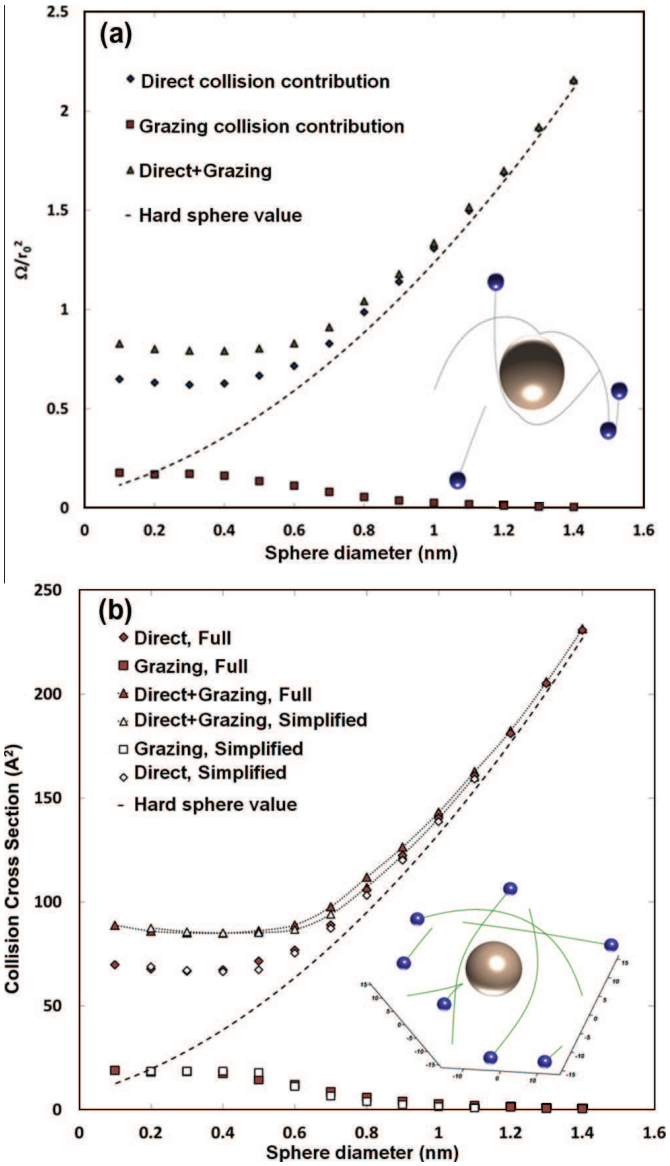

Fig. 8. (a) The normalized collision cross section of a spherical structure in N_2 background gas at 304 K as a function of sphere diameter as determined from DTM calculations. The contributions of both direct and grazing collisions to the collision cross section are shown. (b) A comparison of collision cross section calculated for a sphere in N_2 background gas at 304 K with the full velocity distribution function as well as the simplified velocity distribution function used in DTM calculations.

structure size, a gas molecule will collide with any structure when such conditions are met, while for $b^4 > \alpha_{pol} z^2 e^2 / (\pi \varepsilon \varepsilon_0 C_{init}^2 m_{red})$, direct collision between a finite sized spherical structure and a gas molecule only occurs when the sum of the gas molecule and structure radii is less than r_{min}.

Eq. (46) hence provides a means to distinguish grazing from direct collisions. Fig. 7 shows the DTM-determined cosines of the deflection angles of grazing gas molecules (determined from their velocity vectors as they leave the control volume relative to their entering velocity vectors) as functions of $2U_{pol}(r_{min})/(m_{red}C_{init}^2)$, where $U_{pol}(r_{min})$ is the polarization potential calculated at the apsidal distance. Fitting curves are shown for guidance, as are images of the expected trajectories for the gas molecules (about a finite sized spherical particle) for deflection angles of 0, $\pi/2$, π, $3\pi/2$, 2π, $5\pi/2$ and 3π. Clearly evident, the deflection angle for grazing collisions is defined by the gas molecules initial impact parameter and initial speed. This information, and a regression fit for the deflection angles in Fig. 7 are hence input into DTM calculations, such that the trajectories of grazing collisions need not be calculated for singly charged structures; rather, grazing collisions are immediately identified (by circumscribing the structure with a sphere) using the noted inequality, and the momentum transferred to a structure by grazing gas molecules is calculated directly.

3.3.3. Collision cross section enhancement by polarization

With grazing molecules directly accounted for, the collision cross section of a spherical structure of finite radius in N_2 background gas can be determined. Calculations such as these enable determination of the function $\mathscr{L}$ with prescribed scattering rules and, for prescribed structures, the determination of a single function which describes all results would support the approximately validity of Eqs. (2a) and (2b). Fig. 8(a) shows the collision cross section of a singly charged sphere, considering specular scattering, as a function of the sphere diameter (in nanometers). The influence of grazing collisions and direct contact collisions is shown separately, with the total collision cross section determined as the sum of the collision cross sections due to these two collision types. 10 million gas molecules are used for each result point, and reported collision cross sections are normalized by a characteristic length r_0 based on the polarization energy:

$$r_0^2 = \left(\frac{\alpha_{pol} e^2}{12\pi\varepsilon_0 kT} \right)^{1/2}. \tag{47}$$

Noticeable in Fig. 8(a) a limit in collision cross section is reached when the diameter of the sphere reaches approximately 0.4 nm and varies little as the sphere size is decreased below this value. For a temperature of 304 K, Eq. (47) yields a value of 107.32 Å^2 for N_2, and thus the collision cross sectional limit under the calculation conditions is approximately 86 Å^2 (without N_2); lower collision cross sections are not possible, unless the mass of the structure is well below that of the back ground gas molecules (simulations are performed on infinite mass structures).

3.3.4. Simplification of DTM calculations

Even with direct calculation of grazing collision contributions, DTM calculations are still slowed by the need to incorporate the contribution of the general Maxwell distribution, ρ_0, into calculations. The distribution is not simplified mainly because doing so would incorrectly define the trajectories of the incoming gas molecules, particularly for gas molecules that enter from the front or back walls of the control volume, which have velocities of $\mathbf{c} + \mathbf{V}$ and $\mathbf{c} - \mathbf{V}$ respectively and hence behave differently in the presence of potentials. However, if $\mathbf{V}$ is sufficiently small such that it scarcely influences trajectories, then the simplification of the gas molecule velocity distribution employed in DHSS calculations (and in Mason and McDaniel's methods) can be made for DTM calculations as well. With DTM calculations as presented, there already is a restriction on $\mathbf{V}$, as the linearization of the velocity distribution only applies when the bulk speed is substantially smaller than the mean thermal speed. Fig. 8(b) hence compares DTM calculations performed using the full gas molecule velocity distribution function to those performed using the simplified distribution function where the factor $2 * V$ is purposefully omitted from Eqs. (17) and (18) so that the molecules have a reasonable speed for the acting potentials. Calculation conditions are identical to those presented in Fig. 8(a), with Fig. 8(b) having 10 million and 300,000 trajectories used with the full and simplified distributions, respectively. For this particular instance, reasonable agreement is found, suggesting that a simplified distribution function can be used under some circumstances, but caution should be exercised prior to making this simplification.

4. Conclusions

Three methods of collision cross section calculation are proposed, which are distinct from existing methods and can account for the influences of non-specular scattering and the ion-induced dipole potential between incoming gas molecules and a structure. The latter two of these methods, the DHSS and DTM methods, are described in detail and are applied to collision cross section calculations for spheres, quasifractal aggregates, and fullerene-like structures. DHSS and DTM results are then compared to the simple projected area approximation results. Overall, DHSS and DTM results converge to known analytical solutions when tested under the appropriate circumstances, and appear capable of predicting collision cross sections in non-monoatomic gases. Further study utilizing these methods should enable comparison of collision cross section measurements to predicted collision cross sections for structural models of nanoparticle and macromolecular ions [53].

Moreover, continued development of these methods would allow for the inclusion of gas molecule–gas molecule interactions in order to examine momentum transfer at lower Knudsen numbers, at both high and low bulk speeds.

Acknowledgements

This work was supported by NSF Grant CHE-1011810. C.L. also acknowledges support from the Ramon Areces Foundation.

Appendix A. Supplementary data

Supplementary data associated with this article can be found, in the online version, at http://dx.doi.org/10.1016/j.jcp.2013.05.038.

References

[1] E.W. McDaniel, E.A. Mason, The Mobility and Diffusion of Ions in Gases, John Wiley &Sons, Inc., New York, NY, 1973.
[2] D.E. Clemmer, M.F. Jarrold, Ion mobility measurements and their applications to clusters and biomolecules, Journal of Mass Spectrometry 32 (6) (1997) 577–592.
[3] P.R. Kemper, M.T. Bowers, Electronic-state chromatography – application to 1st-row transition-metal ions, Journal of Physical Chemistry 95 (13) (1991) 5134–5146.
[4] J. Fernandez de la Mora, L. de Juan, T. Eichler, J. Rosell, Differential mobility analysis of molecular ions and nanometer particles, Trac-Trends in Analytical Chemistry 17 (6) (1998) 328–339.
[5] H. Tammet, Size and mobility of nanometer particles, clusters and ions, Journal of Aerosol Science 26 (3) (1995) 459–475.
[6] N.D. Loh, C.Y. Hampton, A.V. Martin, D. Starodub, R.G. Sierra, A. Barty, A. Aquila, J. Schulz, L. Lomb, J. Steinbrener, R.L. Shoeman, S. Kassemeyer, C. Bostedt, J. Bozek, S.W. Epp, B. Erk, R. Hartmann, D. Rolles, A. Rudenko, B. Rudek, L. Foucar, N. Kimmel, G. Weidenspointner, G. Hauser, P. Holl, E. Pedersoli, M. Liang, M.M. Hunter, L. Gumprecht, N. Coppola, C. Wunderer, H. Graafsma, F. Maia, T. Ekeberg, M. Hantke, H. Fleckenstein, H. Hirsemann, K. Nass, T.A. White, H.J. Tobias, G.R. Farquar, W.H. Benner, S.P. Hau-Riege, C. Reich, A. Hartmann, H. Soltau, S. Marchesini, S. Bajt, M. Barthelmess, P. Bucksbaum, K.O. Hodgson, L. Struder, J. Ullrich, M. Frank, I. Schlichting, H.N. Chapman, M.J. Bogan, Fractal morphology, imaging and mass spectrometry of single aerosol particles in flight, Nature 486 (7404) (2012) 513–517.
[7] P. Langevin, Une formule fondamentale de theorie cinetique, Annales de Chimie et de Physique 5 (1905) 215–288.
[8] E. Cunningham, On the velocity of steady fall of spherical particles through fluid medium, Proceedings of the Royal Society of London. Series A 83 (563) (1910) 357–365.
[9] P.L.W. Weick, H.F. Mayer, Über Elektrizitätsleitung durch freie Elektronen und Träger. III: Wanderungsgeschwindigkeit kraftgetriebener Partikel in reibenden Medien, Annalen der Physik 366 (665–741) (1920).
[10] P.S. Epstein, On the resistance experienced by spheres in their motion through gases, Physical Review 23 (1924) 710–733.
[11] R.A. Millikan, A new modification of the cloud method of determining the elementary electrical charge and the most probable value of that charge, Philosophical Magazine 19 (1910) 209–228.
[12] R.A. Millikan, The general law of fall of a small spherical body through a gas, and its bearing upon the nature of molecular reflection from surfaces, Physical Review 22 (1923) 1–23.
[13] M.F. Mesleh, J.M. Hunter, A.A. Shvartsburg, G.C. Schatz, M.F. Jarrold, Structural information from ion mobility measurements: effects of the long-range potential, Journal of Physical Chemistry 100 (40) (1996) 16082–16086.
[14] J.H. Kim, G.W. Mulholland, S.R. Kukuck, D.Y.H. Pui, Slip correction measurements of certified PSL nanoparticles using a nanometer differential mobility analyzer (nano-DMA) for Knudsen number from 0.5 to 83, Journal of Research of the National Institute of Standards and Technology 110 (1) (2005) 31–54.
[15] M.D. Allen, O.G. Raabe, Slip correction measurements of spherical solid aerosol-particles in an improved millikan apparatus, Aerosol Science and Technology 4 (1985) 269–286.
[16] B.K. Ku, J. Fernandez de la Mora, D.A. Saucy, J.N. Alexander, Mass distribution measurement of water-insoluble polymers by charge-reduced electrospray mobility analysis, Analytical Chemistry 76 (3) (2004) 814–822.
[17] D.A. Saucy, S. Ude, I.W. Lenggoro, J. Fernandez de la Mora, Mass analysis of water-soluble polymers by mobility measurement of charge-reduced ions generated by electrosprays, Analytical Chemistry 76 (4) (2004) 1045–1053.
[18] C.J. Hogan, J. Fernandez de la Mora, Tandem ion mobility-mass spectrometry (IMS-MS) study of ion evaporation from ionic liquid-acetonitrile nanodrops, Physical Chemistry Chemical Physics 11 (36) (2009) 8079–8090.
[19] B.K. Ku, J. Fernandez de la Mora, Relation between electrical mobility, mass, and size for nanodrops 1–6.5 nm in diameter in air, Aerosol Science and Technology 43 (3) (2009) 241–249.
[20] C. Larriba, C.J. Hogan, M. Attoui, R. Borrajo, J. Fernandez-Garcia, J. Fernandez de la Mora, The mobility-volume relationship below 3.0 nm examined by tandem mobility-mass measurement, Aerosol Science and Technology 45 (2011) 453–467.
[21] J.M. Eglin, The coefficients of viscosity and slip of carbon dioxide by the oil drop method and the law of motion of an oil drop in carbon dioxide, oxygen, and helium, at low pressures, Physical Review 22 (1923) 161–170.
[22] D.G. Rader, Momentum slip correction factor for small particles in 9 common gases, Journal of Aerosol Science 21 (1990) 161–168.
[23] P. Chan, B. Dahneke, Free-molecule drag on straight chains of uniform sphere, Journal of Applied Physics 52 (1981) 3106–3110.
[24] P. Garcia-Ybarra, D.E. Rosner, Thermophoretic properties of nonspherical particles and large molecules, AIChE Journal 35 (1989) 139–147.
[25] D.E. Rosner, D.W. Mackowski, P. Garcia-Ybarra, Size-insensitivity and structure-insensitivity of the thermophoretic transport of aggregated soot particles in gases, Combustion Science and Technology 80 (1–3) (1991) 87–101.
[26] P. Meakin, B. Donn, G.W. Mulholland, Collisions between point masses and fractal aggregates, Langmuir 5 (1989) 510–518.
[27] J. Fernandez de la Mora, Free-molecule mobility of polyhedra and other convex hard-bodies, Journal of Aerosol Science 33 (3) (2002) 477–489.
[28] M. Zurita-Gotor, Size- and structure-independence of the thermophoretic transport of an aerosol particle for specular boundary conditions in the free molecule regime, Journal of Aerosol Science 37 (3) (2006) 283–291.
[29] S. Chapman, T.G. Cowling, The Mathematical Theory of Non-uniform Gases, Cambridge University Press, Cambridge, UK, 1991.
[30] R. Nakamura, Y. Hidaka, Free molecular gas drag on fluffy aggregates, Astronomy and Astrophysics 340 (1998) 329–334.
[31] D.W. Mackowski, Monte Carlo simulation of hydrodynamic drag and thermophoresis of fractal aggregates of spheres in the free-molecule flow regime, Journal of Aerosol Science 37 (2006) 242–259.
[32] E.A. Mason, E.W. McDaniel, Transport Properties of Ions in Gases, Wiley, New York, 1988.
[33] Z. Li, H. Wang, Drag force, diffusion coefficient, and electric mobility of small particles. I. Theory applicable to the free-molecule regime, Physical Review E 68 (2003) 061206.
[34] Z. Li, H. Wang, Drag force, diffusion coefficient, and electric mobility of small particles. II. Application, Physical Review E 68 (2003) 061207.

[35] V.Y. Rudyak, S.L. Krasnolutski, in: L.J.F. Hermans, B. Nagels, P. Bakker (Eds.), Proceedings of the XXI International Symposium on Rarefied Gas Dynamics, Marseille, Toulouse, France, 1999.
[36] A.A. Shvartsburg, M.F. Jarrold, An exact hard-spheres scattering model for the mobilities of polyatomic ions, Chemical Physics Letters 261 (1–2) (1996) 86–91.
[37] A.A. Shvartsburg, S.V. Mashkevich, E.S. Baker, R.D. Smith, Optimization of algorithms for ion mobility calculations, Journal of Physical Chemistry A 111 (10) (2007) 2002–2010.
[38] B.S. Kinnear, D.T. Kaleta, M. Kohtani, R.R. Hudgins, M.F. Jarrold, Conformations of unsolvated valine-based peptides, Journal of the American Chemical Society 122 (38) (2000) 9243–9256.
[39] A.A. Shvartsburg, G.C. Schatz, M.F. Jarrold, Mobilities of carbon cluster ions: critical importance of the molecular attractive potential, Journal of Chemical Physics 108 (6) (1998) 2416–2423.
[40] J. Jiang, J. Zhao, M. Chen, F. Eisele, J.H. Scheckman, B.J. Williams, C. Kuang, P.H. McMurry, First measurements of neutral atmospheric cluster and 1–2 nm particle number size distributions during nucleation events, Aerosol Science and Technology 45 (2011) ii–v.
[41] B.T. Ruotolo, J.L.P. Benesch, A.M. Sandercock, S.J. Hyung, C.V. Robinson, Ion mobility-mass spectrometry analysis of large protein complexes, Nature Protocols 3 (7) (2008) 1139–1152.
[42] T. Beitz, R. Laudien, H.-G. Löhmannsröben, B. Kallies, Ion mobility spectrometric investigation of aromatic cations in the gas phase, The Journal of Physical Chemistry A 110 (10) (2006) 3514–3520.
[43] C.A. Scarff, K. Thalassinos, G.R. Hilton, J.H. Scrivens, Travelling wave ion mobility mass spectrometry studies of protein structure: biological significance and comparison with X-ray crystallography and nuclear magnetic resonance spectroscopy measurements, Rapid Communications in Mass Spectrometry 22 (20) (2008) 3297–3304.
[44] H.I. Kim, H. Kim, E.S. Pang, E.K. Ryu, L.W. Beegle, J.A. Loo, W.A. Goddard, I. Kanik, Structural characterization of unsaturated phosphatidylcholines using traveling wave ion mobility spectrometry, Analytical Chemistry 81 (20) (2009) 8289–8297.
[45] I. Campuzano, M.F. Bush, C.V. Robinson, C. Beaumont, K. Richardson, H. Kim, H.I. Kim, Structural characterization of drug-like compounds by ion mobility mass spectrometry: comparison of theoretical and experimentally derived nitrogen collision cross sections, Analytical Chemistry 84 (2) (2012) 1026–1033.
[46] H. Kim, H.I. Kim, P.V. Johnson, L.W. Beegle, J.L. Beauchamp, W.A. Goddard, I. Kanik, Experimental and theoretical investigation into the correlation between mass and ion mobility for choline and other ammonium cations in N-2, Analytical Chemistry 80 (6) (2008) 1928–1936.
[47] C. Zhang, T. Thajudeen, C. Larriba, T.E. Schwartzentruber, C.J. Hogan, Determination of the scalar friction factor for non-spherical particles and aggregates across the entire Knudsen number range by direct simulation Monte Carlo (DSMC), Aerosol Science and Technology 46 (2012) 1065–1078.
[48] R. Gopalakrishnan, T. Thajudeen, C.J. Hogan, Collision limited reaction rates for arbitrarily shaped particles across the entire diffusive Knudsen number range, Journal of Chemical Physics 135 (2011) 054302.
[49] T. Thajudeen, R. Gopalakrishnan, C.J. Hogan, The collision rate of non-spherical particles and aggregates for all diffusive Knudsen numbers, Aerosol Science and Technology 46 (2012) 1174–1186.
[50] C. Bleiholder, T. Wyttenbach, M.T. Bowers, A novel projection approximation algorithm for the fast and accurate computation of molecular collision cross sections (I). Method, International Journal of Mass Spectrometry 308 (1) (2011) 1–10.
[51] M. Zurita-Gotor, D.E. Rosner, Effective diameters for collisions of fractal-like aggregates: recommendations for improved aerosol coagulation frequency predictions, Journal of Colloid and Interface Science 255 (1) (2002) 10–26.
[52] E. van Duijn, A. Barendregt, S. Synowsky, C. Versluis, A.J.R. Heck, Chaperonin complexes monitored by ion mobility mass spectrometry, Journal of the American Chemical Society 131 (4) (2009) 1452–1459.
[53] C. Larriba, C.J. Hogan, Ion Mobilities in Diatomic Gases: Measurement versus Prediction with Non-Specular Scattering Models, Journal of Physical Chemistry A 117 (2013) 3887–3901.
[54] A.J. Borysik, C.V. Robinson, The 'sticky business' of cleaning gas-phase membrane proteins: a detergent oriented perspective, Physical Chemistry Chemical Physics 14 (42) (2012) 14439–14449.
[55] Z.G. Li, H. Wang, Gas-nanoparticle scattering: a molecular view of momentum accommodation function, Physical Review Letters 95 (1) (2005) 014502.
[56] J. Happel, H. Brenner, Low Reynolds number hydrodynamics, Martinus Nijhoff Publishers, The Hague, The Netherlands, 1983.
[57] M.P. Allen, D.J. Tildesley, Computer Simulation of Liquids, Oxford Science Publications, 1987.
[58] M. Niwa, K. Yamazaki, Y. Murakami, Separation of oxygen and nitrogen due to the controlled pore-opening size of chemically vapor deposited zeolite A, Industrial & Engineering Chemistry Research 30 (1) (1991) 38–42.
[59] M.M. Maricq, Chemical characterization of particulate emissions from diesel engines: a review, Journal of Aerosol Science 38 (11) (2007) 1079–1118.
[60] M.L. Eggersdorfer, A.J. Gröhn, C.M. Sorensen, P.H. McMurry, S.E. Pratsinis, Mass-mobility characterization of flame-made ZrO_2 aerosols: primary particle diameter and extent of aggregation, Journal of Colloid and Interface Science 387 (1) (2012) 12–23.
[61] C.M. Sorensen, The mobility of fractal aggregates: a review, Aerosol Science and Technology 45 (7) (2011) 765–779.
[62] A.V. Filippov, M. Zurita, D.E. Rosner, Fractal-like aggregates: relation between morphology and physical properties, Journal of Colloid and Interface Science 229 (1) (2000) 261–273.
[63] E.H. Kennard, Kinetic Theory of Gases, McGraw-Hill, 1938.
[64] E.T. Whittake, A Treatise on the Analytical Dynamics of Particles and Rigid Bodies, C.U. Press, 1904.
[65] H. Ouyang, R. Gopalakrishnan, C.J. Hogan, Nanoparticle collisions in the gas phase in the presence of singular contact potentials, Journal of Chemical Physics 137 (2012) 064316.
[66] J.E. Allen, Probe theory – the orbital motion approach, Physica Scripta 45 (5) (1992) 497–503.
[67] N.A. Fuchs, A.G. Sutugin, Coagulation rate of highly dispersed aerosols, Journal of Colloid Science 20 (1965) 492–500.